



UNIVERSITY OF LEEDS

This is a repository copy of *Photoelectron spectroscopy of the hydroxymethoxide anion, H<sub>2</sub>C(OH)O<sup>-</sup>*.

White Rose Research Online URL for this paper:  
<http://eprints.whiterose.ac.uk/111916/>

Version: Accepted Version

---

**Article:**

Oliveira, AM, Lehman, JH [orcid.org/0000-0001-6610-6519](http://orcid.org/0000-0001-6610-6519), McCoy, AB et al. (1 more author) (2016) Photoelectron spectroscopy of the hydroxymethoxide anion, H<sub>2</sub>C(OH)O<sup>-</sup>. The Journal of Chemical Physics, 145 (12). 124317. ISSN 0021-9606

<https://doi.org/10.1063/1.4963225>

---

© 2016, the Author(s). This article may be downloaded for personal use only. Any other use requires prior permission of the author and AIP Publishing. The following article appeared in Oliveira, AM, Lehman, JH , McCoy, AB et al. (1 more author) (2016) Photoelectron spectroscopy of the hydroxymethoxide anion, H<sub>2</sub>C(OH)O<sup>-</sup>. The Journal of Chemical Physics, 145 (12). 124317. ISSN 0021-9606 and may be found at <https://doi.org/10.1063/1.4963225>.

**Reuse**

Unless indicated otherwise, fulltext items are protected by copyright with all rights reserved. The copyright exception in section 29 of the Copyright, Designs and Patents Act 1988 allows the making of a single copy solely for the purpose of non-commercial research or private study within the limits of fair dealing. The publisher or other rights-holder may allow further reproduction and re-use of this version - refer to the White Rose Research Online record for this item. Where records identify the publisher as the copyright holder, users can verify any specific terms of use on the publisher's website.

**Takedown**

If you consider content in White Rose Research Online to be in breach of UK law, please notify us by emailing [eprints@whiterose.ac.uk](mailto:eprints@whiterose.ac.uk) including the URL of the record and the reason for the withdrawal request.



[eprints@whiterose.ac.uk](mailto:eprints@whiterose.ac.uk)  
<https://eprints.whiterose.ac.uk/>

## Photoelectron Spectroscopy of the Hydroxymethoxide Anion, $\text{H}_2\text{C}(\text{OH})\text{O}^-$

Allan M. Oliveira<sup>1</sup>, Julia H. Lehman<sup>1</sup>, Anne B. McCoy<sup>2</sup> and W. Carl Lineberger<sup>1</sup>

<sup>1</sup>JILA and Department of Chemistry and Biochemistry, University of Colorado, Boulder, Colorado 80309

<sup>2</sup>Department of Chemistry, University of Washington, Seattle, Washington 98195

### Abstract

We report the negative ion photoelectron spectroscopy of the hydroxymethoxide anion,  $\text{H}_2\text{C}(\text{OH})\text{O}^-$ . The photoelectron spectra show that 3.49 eV photodetachment produces two distinct electronic states of the neutral hydroxymethoxy radical ( $\text{H}_2\text{C}(\text{OH})\text{O}^\bullet$ ). The  $\text{H}_2\text{C}(\text{OH})\text{O}^\bullet$  ground state ( $\tilde{X}^2A$ ) photoelectron spectrum exhibits a vibrational progression consisting primarily of the OCO symmetric and asymmetric stretches, the OCO bend, as well as combination bands involving these modes with other, lower frequency modes. A high-resolution photoelectron spectrum aids in the assignment of several vibrational frequencies of the neutral  $\text{H}_2\text{C}(\text{OH})\text{O}^\bullet$  radical, including an experimental determination of the  $\text{H}_2\text{C}(\text{OH})\text{O}^\bullet$   $2\nu_{12}$  overtone of the H-OCO torsional vibration as  $220(10) \text{ cm}^{-1}$ . The electron affinity of  $\text{H}_2\text{C}(\text{OH})\text{O}^-$  is determined to be  $2.220(2) \text{ eV}$ . The low-lying  $\tilde{A}^2A$  excited state is also observed, with a spectrum that peaks  $\sim 0.8 \text{ eV}$  above the  $\tilde{X}^2A$  state origin. The  $\tilde{A}^2A$  state photoelectron spectrum is a broad, partially resolved band. Quantum chemical calculations and photoelectron simulations aid in the interpretation of the photoelectron spectra. In addition, the gas phase acidity of methanediol is calculated to be  $366(2) \text{ kcal mol}^{-1}$ , which results in an OH bond dissociation energy,  $D_0(\text{H}_2\text{C}(\text{OH})\text{O}-\text{H})$ , of  $104(2) \text{ kcal mol}^{-1}$ , using the experimentally determined electron affinity of the hydroxymethoxy radical.

## I. Introduction

Alkoxy radicals are known to play an important role in tropospheric and combustion chemistry.<sup>1-7</sup> Many experimental and theoretical studies have focused on the effects of adding various substituents onto the methoxy radical, the simplest alkoxy radical, looking for trends in tropospheric reaction kinetics, unimolecular processes, and overall reactivity.<sup>1-5,8</sup> The hydroxymethoxy radical ( $\text{H}_2\text{C}(\text{OH})\text{O}^\bullet$ ) is an oxygenated alkoxy radical, proposed to be formed from the UV photofragmentation of hydroxymethyl hydroperoxide ( $\text{H}_2\text{C}(\text{OH})\text{OOH}$ ), a product from the tropospheric oxidation of alkenes.<sup>9-13</sup> In addition to the potential atmospheric importance of the  $\text{H}_2\text{C}(\text{OH})\text{O}^\bullet$  radical, its corresponding anion, hydroxymethoxide ( $\text{H}_2\text{C}(\text{OH})\text{O}^-$ ), is the conjugate base of methanediol ( $\text{H}_2\text{C}(\text{OH})_2$ ), considered to be a molecule of astrochemical and possible prebiotic relevance<sup>14-18</sup> as a building block of simple amino acids.<sup>19,20</sup> Despite the relevance of the hydroxymethoxy radical to combustion and planetary chemistry, very little is known about its spectroscopy. In fact,  $\text{H}_2\text{C}(\text{OH})\text{O}^\bullet$  has only recently been experimentally observed. Cao *et al.*<sup>21</sup> detected  $\text{H}_2\text{C}(\text{OH})\text{O}^\bullet$  as a product from the reaction of atomic hydrogen with formic acid in a krypton matrix isolation experiment. In this experiment, the radical product was only stable for a few hours at the cryogenic matrix temperatures before isomerizing to  $\text{HC}^\bullet(\text{OH})_2$ . In general, the high reactivity of  $\text{H}_2\text{C}(\text{OH})\text{O}^\bullet$  makes a direct gas phase experimental observation very challenging.

The comparison of  $\text{H}_2\text{C}(\text{OH})\text{O}^\bullet$  with other alkoxy radicals is an interesting study on the effects of non-alkyl substituents on the electronic structure of the methoxy radical. Previous experimental and theoretical work studied the effect of methyl substitutions, forming ethoxy, isopropoxy, and *tert*-butoxy radicals.<sup>22-27</sup> The substitution of a methyl group for a hydrogen atom will change the electronic structure of the methoxy radical, breaking its  $C_{3v}$  symmetry. For the ethoxy radical, significant Jahn-Teller distortions were observed in the  $\text{CH}_3\text{CH}_2\text{O}^-$  photoelectron spectrum, where the  $\text{CH}_3\text{CH}_2\text{O}^\bullet \tilde{A}$  state was found to be only  $355 \text{ cm}^{-1}$  higher in energy than the ground  $\tilde{X}$  state.<sup>22</sup> The inclusion of vibronic coupling was imperative in order to analyze its spectrum.<sup>23</sup> There was significantly less vibronic coupling observed for the isopropoxy and *tert*-butoxy radicals.<sup>22,27</sup>

While the work on interpreting the photoelectron spectra of the ethoxide anion yielded results that needed to be analyzed with the inclusion of Jahn-Teller distortions and vibronic coupling,<sup>22,23,25,28</sup> recent calculations suggest this will not be the case for hydroxymethoxy.<sup>26</sup> Eisfeld and Francisco<sup>11</sup> studied low lying electronic states of  $\text{H}_2\text{C}(\text{OH})\text{O}^\bullet$ , focusing on calculating its electronic absorption spectra (CASSCF/CASPT2, CASSCF/MRCI+Q). Although they pointed out that nonadiabatic effects might exist between the low-lying electronic states of  $\text{H}_2\text{C}(\text{OH})\text{O}^\bullet$ , they were not explicitly included in the calculations.<sup>11</sup> Dillon and Yarkony,<sup>26</sup> on the other hand, explored the ground  $\tilde{X}^2A$  and first excited  $\tilde{A}^2A$  electronic states of  $\text{H}_2\text{C}(\text{OH})\text{O}^\bullet$  (SA-MCSCF/MR-SDCI), comparing its electronic structure with other substitutional isomers of the methoxy radical (ethoxy and isopropoxy radicals). This work showed that there are strong nonadiabatic couplings between the ground ( $\tilde{X}^2A$ ) and the first excited ( $\tilde{A}^2A$ ) electronic states of  $\text{H}_2\text{C}(\text{OH})\text{O}^\bullet$ .

This work presents an anion photoelectron spectroscopic investigation of the hydroxymethoxy radical, as well as the measurement of its electron affinity (EA). Here, the ground  $\tilde{X}^2A$  and first excited  $\tilde{A}^2A$  states of  $\text{H}_2\text{C}(\text{OH})\text{O}^\bullet$  are observed through negative ion photoelectron spectroscopy of  $\text{H}_2\text{C}(\text{OH})\text{O}^-$ . The high reactivity of neutral  $\text{H}_2\text{C}(\text{OH})\text{O}^\bullet$  and its close relation to methanediol motivates its spectroscopic investigation through its negative ion,  $\text{H}_2\text{C}(\text{OH})\text{O}^-$ , which is predicted to be more stable by 2.232 eV.<sup>11</sup> A comparison with other small alkoxy radicals is drawn, together with an exploration of the H-OCO torsional motion. Quantum chemical calculations aid in the interpretation of the photoelectron spectra and provide accurate thermochemical quantities of the gas phase chemistry of methanediol.

## II. Methods

### *A. Experimental*

In this experiment, a velocity map imaging (VMI) mass-selected anion photoelectron spectrometer is employed, and has been described in detail previously.<sup>29</sup> Briefly, the experimental apparatus consists of three regions: the ion source, mass separation, and detection regions. The hydroxymethoxide anion is generated from an association reaction between the hydroxide anion ( $\text{OH}^-$ )

and neutral formaldehyde ( $\text{H}_2\text{CO}$ ) using a pulsed plasma entrainment ion source.<sup>30</sup> This source consists of two pulsed General Valves (Parker-Hannifin, Series 9): a primary supersonic expansion (40 psig, ~1%  $\text{H}_2\text{CO}$  in argon) and a low flow secondary expansion (30 psig, 1%  $\text{O}_2$ , 30%  $\text{H}_2$ , balance argon), oriented perpendicularly to the primary expansion. The secondary expansion generates the  $\text{OH}^-$  ions in a pulsed discharge. This plasma is entrained into the main supersonic expansion, which introduces the second reactant ( $\text{H}_2\text{CO}$ ), provides collisional cooling, and stabilizes the generated ions.

In order to produce a mixture of pure formaldehyde in argon, a procedure similar to the one described by Ho *et al.* is followed.<sup>31</sup> Here, a solid sample of polyoxymethylene (formaldehyde polymer) is heated to 60(5) °C under a 40 psig flow of argon. The principal product from the decomposition of polyoxymethylene is gaseous monomeric formaldehyde, but water and other small oligomers, such as dimeric formaldehyde and trioxane, are also formed. This gaseous mixture flows through a glass trap equipped with a fritted glass disk and held at -80 °C (dry ice/methanol bath) in order to trap these undesired products and prevent repolymerization. The vapor pressure of liquid formaldehyde at this temperature is enough to provide a ~0.8% mixture of formaldehyde in argon.<sup>32</sup>

Approximately 20 cm downstream from the primary supersonic expansion nozzle, the negative ions are extracted into a Wiley-McLaren time-of-flight mass spectrometer, where they are accelerated to ~3 keV, separated by their mass-to-charge ( $m/z$ ) ratio, steered, and focused onto an inline microchannel plate (MCP) detector. Using an appropriately timed laser pulse, anions with the desired  $m/z$  are selected for photodetachment at the spatial focus of the Wiley-McLaren mass spectrometer. A horizontally polarized laser pulse creates a small volume of photodetached electrons, which are extracted into a VMI photoelectron spectrometer, perpendicular to the ion trajectory. These photoelectrons are projected onto a 2D position sensitive MCP/phosphor screen detector, coupled to a CCD camera. The resulting 2D photoelectron image is transformed into a photoelectron velocity distribution using the BASEX<sup>33</sup> Abel inversion program or the MEVELER<sup>34</sup> algorithm. The electron velocity is then converted to kinetic energy through a Jacobian transformation, yielding photoelectron spectra as a function of electron kinetic energy (eKE). Since the eKE depends on the wavelength used for photodetachment, the spectra are

reported here as a function of electron binding energy ( $eBE = h\nu - eKE$ ), which is independent of the photon energy.

The energy resolution of the VMI improves with decreasing  $eKE$ , with the best resolution for  $eKE \leq 0.1$  eV, becoming too poor to be really useful in this experiment for  $eKE \geq 1.0$  eV. Therefore, several different photon energies are used, with the combined results providing the reported photoelectron spectra. Specifically, the second and third harmonics of a pulsed Nd:YAG laser (2.33 eV (532 nm) and 3.49 eV (355 nm), respectively), and 2.74 eV (453 nm) from a 355 nm pumped optical parametric oscillator (OPO) were used in the work reported here. The laser light was focused into the ion interaction region using a 0.5 m focal length UV grade fused silica lens. In this experiment, for  $eKE \geq 0.2$  eV, the ratio of the peak full width at half maximum ( $fwhm$ ) to  $eKE$  approaches a constant value of  $fwhm/eKE \sim 3\%$ . The energy scale was calibrated using the known photoelectron spectra of  $S^{-35,36}$  or  $OH^{-}$ .<sup>37</sup>

In addition to the photoelectron kinetic energy distribution, the VMI spectrometer also provides the angular distribution of photoelectrons with respect to the laser polarization. Using the Cooper-Zare relation,<sup>38</sup>  $I(\theta) \propto \left[1 + \frac{1}{2}\beta (3 \cos^2 \theta - 1)\right]$ ,  $-1 \leq \beta \leq 2$ , which describes the photoelectron intensity as a function of the polar angle relative to the laser polarization axis, the observed photoelectron angular distributions can be fit to anisotropy parameters,  $\beta$ . This fitting procedure is implemented in the reconstruction software.<sup>33,34</sup> The  $\beta$  parameter provides information about the angular momentum of the orbital from which the photoelectrons originate, and is a useful tool for identifying different electronic states of the neutral molecule being accessed. For a detailed description of angular distributions in negative ion photoelectron spectroscopy, see the review by Sanov.<sup>39</sup>

## ***B. Theoretical Methods***

In this work, all electronic structure calculations are performed using the Gaussian 09 software package.<sup>40</sup> In order to calculate the photoelectron spectra, geometry optimizations and harmonic frequencies are calculated at the CCSD(T)/aug-cc-pVTZ level of theory for  $H_2C(OH)O^-$ , and ROCCSD(T)/aug-cc-pVTZ for the  $H_2C(OH)O^* \tilde{X}^2A$  state. For the excited  $H_2C(OH)O^* \tilde{A}^2A$  electronic

state, geometry optimizations and frequencies are calculated using CIS/aug-cc-pVTZ, while single point energies were calculated at the EOMCCSD/aug-cc-pVTZ level of theory. The calculated normal modes and structural parameters are input into the PESCAL software package, which calculates Franck-Condon factors (FCF) based on the Sharp-Rosenstock-Chen method with Duschinsky rotations.<sup>41-43</sup> The resulting FCFs are used to generate calculated photoelectron spectra.

When the stationary points on the potential surface for the hydroxymethoxy radical are analyzed, it is found that the minimum energy structure is rotated about the H3-O2-C-O1 torsion angle (see the inset in Fig. 1 for atom labeling), labeled throughout this manuscript as  $\varphi_{\text{HOCO}}$ , by  $\pm 48^\circ$  relative to its value at the minimum on the hydroxymethoxide surface, which is at  $\varphi_{\text{HOCO}} = 0^\circ$ . A dihedral angle of  $0^\circ$  is defined as a planar H-OCO moiety in the *cis*- conformation, as shown in the inset in Fig. 1. Based on this, the minimum for the ground  $\tilde{X}^2A$  state of hydroxymethoxy has  $C_1$  symmetry, while the minimum energy structure of the hydroxymethoxide anion has  $C_s$  symmetry. The lowest energy  $C_s$  symmetry structure on the hydroxymethoxy surface is  $160\text{ cm}^{-1}$  above the minimum energy structure and corresponds to a saddle point on the potential surface. By contrast, the harmonic frequency associated with the H-OCO torsion is  $240\text{ cm}^{-1}$ . Based on the above, it is not expected that this torsion vibration will be well-described by a harmonic treatment evaluated at the potential minimum, as is employed in the PESCAL simulation software. These attributes are also seen for the  $\text{H}_2\text{C}(\text{OH})\text{O}^* \tilde{A}^2A$  state, although a larger energy difference between  $C_1$  and  $C_s$  minima is calculated ( $968\text{ cm}^{-1}$  energy difference,  $375\text{ cm}^{-1}$  harmonic frequency of the H-OCO torsion vibration). This is discussed in more detail in Section IV.A.

To introduce this large amplitude motion into the Franck-Condon simulation, the harmonic wavefunctions for the torsion are replaced by the wavefunctions obtained by solving the one dimensional Schrödinger equation associated with the torsion, described below. The remaining vibrations are treated at the harmonic level, where the normal modes and harmonic frequencies are obtained at the  $C_s$  saddle point structure for hydroxymethoxy. These frequencies, rather than those obtained at the  $C_1$  minimum, are used because the torsion wavefunction for the electronic ground state of  $\text{H}_2\text{C}(\text{OH})\text{O}^*$  has significant amplitude at this higher symmetry geometry, as is seen in Fig. S1. In addition, the higher symmetry of

the  $C_s$  saddle point leads to improved separation of the torsion from the other vibrations in the construction of the normal modes due to the absence of coupling between vibrations of A' and A'' symmetry in the development of the normal modes when the Hamiltonian is expressed in symmetry adapted linear combinations of internal coordinates. This approach is similar to that employed in our earlier study of the photoelectron spectra of  $\text{CHX}_2$ , X = Cl, Br and I, which contained a similar large amplitude vibrational mode.<sup>44</sup>

To obtain the torsion wavefunctions, first a one-dimensional relaxed potential energy surface is evaluated for the hydroxymethoxide anion by varying the  $\varphi_{\text{HOCO}}$  dihedral angle while allowing all other coordinates to relax to their values at the minimum energy configuration. This scan (CCSD(T)/aug-cc-pVTZ) was performed from  $0^\circ$  to  $180^\circ$  with variable increments (see Table S1 in the Supplementary Material for calculated points and corresponding energies). In order to better represent the vertical transition region of the potential, which is sampled in the photodetachment experiment, the neutral surface was constructed by calculating the energies of hydroxymethoxy at the optimized anion geometries, as shown in Fig. 1. These energies were fit to:

$$V(\varphi_{\text{HOCO}}) = A + \sum_{n=1}^5 V_n (1 - \cos(n\varphi_{\text{HOCO}})) \quad (1)$$

where the value of  $A$  provides the energy of hydroxymethoxy at the minimum energy geometry of hydroxymethoxide, *e.g.* the vertical detachment energy. The optimized fit parameters are listed in Table S2 of the Supplementary Material.

The eigenvalues and eigenvectors of this potential were calculated by solving the one dimensional Schrödinger equation based on

$$H = \frac{1}{2} p_{\varphi_{\text{HOCO}}} G_{\varphi_{\text{HOCO}}, \varphi_{\text{HOCO}}}(\varphi_{\text{HOCO}}) p_{\varphi_{\text{HOCO}}} + V(\varphi_{\text{HOCO}}) \quad (2)$$

using a basis of Fourier functions,  $\psi(\varphi_{\text{HOCO}}) = \sqrt{\frac{1}{2\pi}} e^{-iJ\varphi_{\text{HOCO}}}$  with  $J=(-100,100)$ . The  $G_{\varphi_{\text{HOCO}}, \varphi_{\text{HOCO}}}$  term in Eq. (2) was evaluated using the expressions given by Frederick and Woywod,<sup>45</sup> and

fit to an expansion in  $(1 - \cos(n\varphi_{\text{HOCO}}))$ , analogous to Eq. (1). Expanding the G-matrix element allows us to account for the effects of geometry changes in the relaxed scan on the effective mass associated with  $\varphi_{\text{HOCO}}$ . Operationally, the value of  $G_{\varphi_{\text{HOCO}},\varphi_{\text{HOCO}}}$  changes by roughly 5% over the range of  $\varphi_{\text{HOCO}}$ . The expansion coefficients are included in the Supplementary Material. The FCFs were then obtained by evaluating the overlap of the two lowest energy vibrational states on the hydroxymethoxide anion potential surface with vibrational states on the hydroxymethoxy neutral surface for the electronic state of interest. Because of the separate treatment of the H-OCO torsional mode and the remainder of the normal modes of the neutral hydroxymethoxy radical described above, the reported calculated spectrum was obtained by convolving each FCF of the remaining 3N-7 normal modes (obtained with PESCAL) with the spectrum obtained for the torsional transitions. The resulting FCFs were then convoluted with Gaussian functions of varying *fwhm* in order to match the experimental resolution, therefore providing a direct comparison between the calculated and experimental spectra. This procedure was repeated for the  $\text{H}_2\text{C}(\text{OH})\text{O}^* \tilde{A}^2A$  excited state calculations also performed here (CIS/aug-cc-pVTZ geometry optimization and vibrational frequencies, EOMCCSD/aug-cc-pVTZ single point energies). The calculations performed here for the optimized geometries and harmonic frequencies of the anion  $\tilde{X}^1A'$  and neutral  $\tilde{X}^2A$ ,  $\tilde{A}^2A$  states are in good agreement with the ones reported by Eisfeld and Francisco<sup>11</sup> (anion: CCSD(T)/aug-cc-pVQZ, neutral: MRCI+Q/aug-cc-pVQZ) and Dillon and Yarkony (SA-MCSCF/MR-SDCI).<sup>26</sup>

### III. Results

Following the ion generation procedure described in Section II.A, an anion with  $m/z = 47$  was successfully produced. Although  $\text{H}_2\text{C}(\text{OH})\text{O}^-$  is the most stable product with  $m/z = 47$  from the association reaction of  $\text{OH}^-$  with  $\text{H}_2\text{CO}$ ,<sup>46</sup> other structural isomers of  $\text{CH}_3\text{O}_2^-$  could exist in the ion beam. However, the use of photoelectron spectroscopy can unequivocally identify the presence or absence of these other isomers. The photoelectron spectrum of methyl hydroperoxide ( $\text{H}_3\text{COO}^-$ ) was reported previously by Blanksby *et al.*,<sup>47</sup> and does not match the reported spectrum here. The other possible

isomers at  $m/z = 47$  are  $\text{H}_2\text{COOH}^-$  and  $\text{HC}(\text{OH})_2^-$ . Based on electronic structure calculations,  $\text{H}_2\text{COOH}^-$  is unstable with respect to isomerization to  $\text{H}_2\text{C}(\text{OH})\text{O}^-$  when calculated at B3LYP/aug-cc-pVTZ level of theory/basis. The other possible structural isomer,  $\text{HC}(\text{OH})_2^-$ , is also unlikely, due to the calculated electron affinity of  $\text{HC}(\text{OH})_2$  being negative (-0.011 eV, B3LYP/aug-cc-pVTZ).

### ***A. Experimental Photoelectron Spectra and $EA(\text{H}_2\text{C}(\text{OH})\text{O}^-)$***

The photoelectron spectrum taken with 3.49 eV photon energy is shown in the middle panel of Fig. 2. The spectrum shows two distinct regions: a structured, regularly spaced progression ranging from 2.2 to 2.7 eV; and a broader, partially resolved peak which spans from  $\sim 2.8$  to 3.5 eV. The top panel of Fig. 2 shows the anisotropy parameter  $\beta$  as a function of eKE (top horizontal axis). The  $\beta$  parameter has a positive value ( $\beta = +0.3(2)$ ) for the broad, high eBE peak, while peaks A–D show increasingly negative  $\beta$  values, where peak A has  $\beta = -0.65(6)$ . Generally,<sup>39</sup> a positive  $\beta$  is associated with a photoelectron originating from an anion molecular orbital with more s-character, while a negative  $\beta$  is associated with photodetachment from an anion molecular orbital with more p-character. A quantitative determination of the fractional s or p character of these anion molecular orbitals is unable to be extracted from this experiment. However, the difference between the photoelectron angular distributions indicates that the two regions of the spectrum can be associated with detachment to form two different electronic states of neutral hydroxymethoxy radical. Using a simple symmetry-based analysis, a transition from the anion HOMO ( $a''$  symmetry orbital) is associated with a negative  $\beta$ , while a transition from the anion HOMO-1 ( $a'$  symmetry) is associated with a positive  $\beta$ .<sup>48</sup> The ground and first excited states of  $\text{CH}_2(\text{OH})\text{O}^\bullet$ , using the  $C_s$  symmetry labels valid at  $\phi_{\text{HOCO}} = 0^\circ$ , are described by  $\tilde{X}^2A''$  and  $\tilde{A}^2A'$  state labels. The molecular orbitals associated with the two lowest energy electronic states of  $\text{H}_2\text{C}(\text{OH})\text{O}^-$  have also already been calculated,<sup>11,26</sup> and are associated with a half-filled  $a''$  ( $a'$ ) symmetry  $p_y$  ( $p_x$ ) orbital at the O1 atom for the ground (excited) electronic state (note: in this representation, the heavy atoms are taken to lie in the  $xz$  plane). Thus, the electron angular anisotropy is consistent with electron detachment from  $\text{H}_2\text{C}(\text{OH})\text{O}^- \tilde{X}^2A''$  to form  $\text{H}_2\text{C}(\text{OH})\text{O}^\bullet \tilde{X}^2A''$  and  $\tilde{A}^2A'$  states (using  $C_s$  symmetry labels). In addition to the evidence

provided by the sign of the angular anisotropy parameter, the calculated term energy ( $T_0$ ) of the lowest lying excited  $\text{H}_2\text{C}(\text{OH})\text{O}^* \tilde{A}^2A$  state puts it approximately 0.38 eV higher in energy than the ground ( $\tilde{X}^2A$ ) state.<sup>11,26</sup> This value is in good agreement with the energy difference between the origins of the two features in Fig. 2. Higher lying excited states exist for  $\text{H}_2\text{C}(\text{OH})\text{O}^*$ , but all are calculated to lie more than 3.5 eV above the ground  $\tilde{X}^2A$  state and should not be candidates for this progression.<sup>11</sup> Thus it is most likely that the higher energy electronic state that is observed is the excited  $\text{H}_2\text{C}(\text{OH})\text{O}^* \tilde{A}^2A$  state.

The lowest eBE peak in the spectrum, peak A, has a *fwhm* of 0.036 eV, a value close to the experimental resolution, suggesting minimal rotational broadening. See Section II.A for more details. Surprisingly, all other peaks in the spectrum are considerably broader despite having lower eKE. This indicates that there are other contributions to the observed width. The  $\tilde{A}^2A$  excited state peak is located at the high eBE (low eKE) region, where an isolated peak at eKE  $\sim 0.5$  eV would be expected to have a width of  $\sim 15$  meV. The fact that no sharp peaks are observed in the  $\tilde{A}^2A$  state, particularly at the high binding energy edge of the spectrum, suggests that there is likely a large degree of spectral congestion in this region of the spectrum (discussed further in Section III.C). The  $\tilde{X}^2A$  ground state progression, on the other hand, also exhibits increasingly broad peaks regularly spaced by  $\sim 0.14$  eV ( $1130 \text{ cm}^{-1}$ ) as the eKE is decreased (eBE is increased). This suggests that peaks B through D consist of multiple vibrational transitions, which are not resolved at this eKE. Therefore, the use of a lower photon energy for photodetachment, yielding a lower eKE spectrum, should reduce the peak widths and provide a more structured spectrum of the  $\tilde{X}^2A$  state of hydroxymethoxy radical.

The photoelectron spectrum of hydroxymethoxide obtained with 2.737 eV photons (453 nm) is shown in the top panel of Fig. 3. The peak labels shown in Fig. 3 are the same as the ones shown in Fig. 2. This spectrum shows more resolved structure compared to the initial low resolution photoelectron spectrum from Fig. 2. Indeed, peaks B-D show additional resolved structure compared to those peaks in Fig. 2. Peak A now has a *fwhm* = 0.018 eV (*fwhm*/eKE = 3.5%); a factor of 2 improvement in absolute peak width when compared to the same peak in Fig. 2. In order to fully resolve the origin transition (peak

A) and accurately determine the EA of  $\text{H}_2\text{C}(\text{OH})\text{O}^\bullet$ , an even lower eKE (therefore higher resolution) photoelectron spectrum using 2.33 eV photon energy is obtained.

The high resolution photoelectron spectrum taken with 2.33 eV photons (532 nm) is shown in the top panel of Fig. 4. This spectrum shows peak A with  $fwhm = 0.008$  eV; another factor of two improvement in peak width when compared to the same peak in Fig. 3. Because the transitions that compose peak A are now clearly resolved, the peaks are relabeled with lowercase letters for individual assignments. Figure 4 shows a clear origin of the vibrational progression centered at 2.2205 eV (peak a), which corresponds to the transition from the ground vibrational state of the  $\text{H}_2\text{C}(\text{OH})\text{O}^-$  anion to the ground vibrational state of the neutral  $\text{H}_2\text{C}(\text{OH})\text{O}^\bullet \tilde{X}^2A$  radical. After a small shift to correct for an unresolved rotational envelope<sup>49</sup> (see Supplementary Material), and inclusion of the uncertainties associated with the measurement, the EA of the hydroxymethoxy radical is assigned as 2.220(2) eV. This agrees very well with the calculated EA from this work (2.19 eV) and with that from a higher level (multireference) calculation (2.232 eV).<sup>11</sup> The uncertainty on the EA and the vibrational frequencies reported below come primarily from the energy scale calibration (see Supplementary Material for a detailed description of how the uncertainties are obtained).

### ***B. $\text{H}_2\text{C}(\text{OH})\text{O}^\bullet \tilde{X}^2A$ Vibrational Assignments***

The  $\text{H}_2\text{C}(\text{OH})\text{O}^\bullet \tilde{X}^2A$  vibrational progression, depicted in Fig. 3, is characterized by an intense origin transition, followed by a progression of decreasing intensity and increasing congestion. Based on the changes in geometry between the anion and neutral equilibrium structures (see Table 1), which shows the largest changes occurring in the  $\angle_{\text{O}_1\text{CO}_2}$  and  $\angle_{\text{H}_3\text{O}_2\text{C}}$  angles and  $r_{\text{CO}_2}$  bond length, one might expect the most active vibrations to consist of OCO and HOC bends, symmetric and asymmetric OCO stretching vibrations, and combination bands involving these vibrations. The calculated photoelectron spectrum (lower panels of Figs. 3 and 4) indeed shows that the ground  $\tilde{X}^2A$  state progression (features A-D) is composed primarily of the vibrations  $\nu_{11}$  (OCO bend),  $\nu_9$  (OCO symmetric stretch),  $\nu_8$  (OCO asymmetric stretch),  $\nu_5$  (out of phase HOC bending/ $\text{CH}_2$  wagging), and  $\nu_4$  (HCH bend). See Supplementary Material

for the description of the molecular motion associated with all modes. In fact, the center of peaks A-D are separated (on average) by  $\sim 0.14$  eV ( $1130$   $\text{cm}^{-1}$ ), which roughly corresponds to the OCO asymmetric stretching vibration ( $\nu_8$ ). The H-OCO torsion vibration ( $\nu_{12}$ ) is also active, and will be discussed in detail in Section IV.A below. Eisfeld and Francisco<sup>11</sup> report extensive calculations on the hydroxymethoxy radical and include a simulated photoelectron spectrum of the anion accessing the ground  $\tilde{X}^2A$  state of the neutral, but not including the HOCO torsional mode. In spite of the fact that the reported geometries and frequencies of the anion and neutral ground  $\tilde{X}^2A$  state are very similar to the current work, the previous photoelectron spectrum simulation produces an extended vibrational progression, spanning close to 2 eV. The overall simulated photoelectron spectrum reported here is in excellent agreement with the experimentally observed spectrum and so it is used as an aid in order to assign the various vibrational transitions responsible for the dominant peaks in the structured photoelectron spectrum shown in Figs. 3 and 4.

The spectral congestion apparent in peaks C and D in Fig. 3, and confirmed by the photoelectron spectrum simulation, makes individual transitions within these peaks impossible to assign. However, peak B appears to be much less congested, and based on the experimental spectrum, peak B in Fig. 3 appears to consist of four peaks. The calculated spectrum shows that five transitions are primarily responsible for the structure in peak B, namely transitions from the ground vibrational level of the anion to one quanta each of modes  $\nu_9$ ,  $\nu_8$ ,  $\nu_6$ ,  $\nu_5$  and  $\nu_4$  (labeled in Fig. 3). The transitions to the fundamentals in  $\nu_9$  and  $\nu_8$ , which correspond to the OCO symmetric and asymmetric stretches, respectively, are in a region where the spectral congestion is minimal and show very good agreement with experiment. Consequently, these transitions are unequivocally assigned, and the observed frequencies, calculated from the difference between the peak positions and the origin (EA) position, are presented in Table 2. The assignments of the  $\nu_6$ ,  $\nu_5$  and  $\nu_4$  fundamentals are not made due to the larger degree of spectral congestion.

The higher resolution spectrum presented in Fig. 4 has six labeled peaks, all of which are captured in the photoelectron simulation. From this spectrum, in addition to obtaining an accurate EA( $\text{H}_2\text{C}(\text{OH})\text{O}^\bullet$ ), transitions to the lowest frequency active modes are resolved, namely the OCO bending

vibration ( $\nu_{11}$ ), the H-OCO torsion vibration ( $\nu_{12}$ ), and a few combination bands. Peak d can now be assigned as the transition from the ground vibrational level of the anion to the state on the neutral potential with one quantum of excitation in the OCO bend. Peaks b and a' are assigned to transitions involving the H-OCO torsion, namely  $\nu_{12}(\nu''=0 \rightarrow \nu'=2)$  and  $\nu_{12}(\nu''=1 \rightarrow \nu'=1)$ , which is further discussed in Section IV.A. Throughout this manuscript, primes (double primes) are used to denote vibrational levels in the neutral (anion) electronic state. The peak positions (absolute eBE and relative to the EA) for the peaks labeled in Figs. 3 and 4 are given in Table S6.

### C. $\text{H}_2\text{C}(\text{OH})\text{O}^* \tilde{A}^2A$

Photoelectron detachment to form  $\text{H}_2\text{C}(\text{OH})\text{O}^* \tilde{A}^2A$  results in a relatively unstructured photoelectron spectrum (Fig. 2), peaked at  $\sim 3$  eV with a *fwhm* of  $\sim 0.5$  eV. As mentioned previously, since there is an approximately constant resolution (*fwhm*/eKE) of 3%, the narrowest peaks should be at low kinetic energy (large binding energy), meaning that detachment to the  $\tilde{A}^2A$  excited state should be the best resolved in this spectrum. This is not what is observed, which implies that photodetachment to the  $\tilde{A}^2A$  excited state could result in a large degree of spectral congestion.

In order to test this hypothesis, a photoelectron spectrum simulation based on excitation to the  $\tilde{A}^2A$  state of  $\text{H}_2\text{C}(\text{OH})\text{O}^*$  was calculated using the methods described above. Based on the measured EA( $\text{H}_2\text{C}(\text{OH})\text{O}^*$ ) and the calculated  $T_0$  of  $\text{H}_2\text{C}(\text{OH})\text{O}^* \tilde{A}^2A$  ( $0.377 \text{ eV}^{26}$  or  $0.390 \text{ eV}^{11}$  with respect to  $\text{H}_2\text{C}(\text{OH})\text{O}^* \tilde{X}^2A$ ), the origin of the excited  $\tilde{A}^2A$  state was initially assumed to be approximately 2.6 eV. The resulting photoelectron spectrum simulation is shown in Fig. 2 (bottom panel) and in the Supplementary Material (Fig. S4). The spectrum shows a large degree of spectral congestion, primarily involving transitions to overtones and combination bands of the H-OCO torsion ( $\nu_{12}$ ), OCO asymmetric stretching ( $\nu_9$ ), and out-of-phase HOC bending/ $\text{CH}_2$  wagging ( $\nu_5$ ) vibrations. The simulated spectrum peaks  $\sim 0.3$  eV above the origin, and extends for at least another 1 eV. Since the experimental photon energy used is only 3.49 eV, the simulated spectrum shown in the lower panel of Fig. 2 is truncated at 3.49 eV. In addition, a threshold scaling factor<sup>50,51</sup> is introduced to help mimic the low eKE edge of the

observed spectrum. Given that the experimentally observed positive anisotropy indicates this excited  $\tilde{A}^2A$  electronic state is a result of electron detachment from an orbital with relatively more s-like character than when the electron is detached to form the ground  $\tilde{X}^2A$  state of  $\text{H}_2\text{C}(\text{OH})\text{O}^*$ , the outgoing electron is approximated by a p-wave. Thus, the photodetachment cross section scales as  $e\text{KE}^{l+0.5}$ , or  $e\text{KE}^{1.5}$ . This means that there is a much stronger threshold effect for the onset of the excited  $\tilde{A}^2A$  state compared to the ground  $\tilde{X}^2A$  state. This scaling factor for the detachment cross section is also consistent with why there are no observed peaks that can be unequivocally assigned to the origin of the excited  $\tilde{A}^2A$  state spectrum in the low eKE region of the 453 nm spectrum.

The overall photoelectron simulation matches the experimental spectrum very well, despite the harmonic treatment and assumption of separable vibrational modes, both of which likely results in undercounting the density of states on the  $\tilde{A}^2A$  potential surface. There is a repeating pattern of peaks in the simulation, spaced by  $\sim 1200\text{ cm}^{-1}$  (0.15 eV, or approximately one quanta of the neutral  $\nu_9$  vibration), which is a result of overtones in the OCO asymmetric stretching ( $\nu_9$ ) and HOC bending/ $\text{CH}_2$  wagging ( $\nu_5$ ) vibrations. Because the origin of the  $\text{H}_2\text{C}(\text{OH})\text{O}^* \tilde{A}^2A$  state is obscured by transitions from the anion to high lying vibrations in the  $\text{H}_2\text{C}(\text{OH})\text{O}^* \tilde{X}^2A$  state, there is some uncertainty in the spectrum's origin, shown in Fig. 2 as 2.615 eV to best match the experimental spectrum while still remaining close to the calculated origin. The calculated spectrum could just as easily shift by  $\pm 0.15\text{ eV}$ , which is the spacing of the repeating pattern of peaks in the simulation, and still match the overall experimental spectrum. However, a shift this large seems unlikely, given the high level multireference calculations of the  $\text{H}_2\text{C}(\text{OH})\text{O}^* \tilde{A} - \tilde{X}$  term energy.<sup>11,26</sup>

## IV. Discussion

### A. H-OCO Torsion

The relaxed H-OCO torsional potential energy surfaces for the anion and neutral ground  $\tilde{X}^2A$  and excited  $\tilde{A}^2A$  states can be found in Fig. 1 and in the Supplementary Material (Figs. S1-S2 and Tables S1

and S2). As mentioned in Section II.B, the  $\tilde{X}^2A$  state of the anion has its minimum energy geometry at  $\phi_{\text{HOCO}} = 0^\circ$ . Although there is a higher energy minimum in the *trans* H-OCO configuration ( $\phi_{\text{HOCO}} = 180^\circ$ ,  $\sim 1200 \text{ cm}^{-1}$  relative to the global minimum), the barrier to conversion from the *trans* to *cis* configurations is too low (on the order of  $20 \text{ cm}^{-1}$ ) to support any bound vibrational levels. For both the ground  $\tilde{X}^2A$  and excited  $\tilde{A}^2A$  states of  $\text{H}_2\text{C}(\text{OH})\text{O}^\bullet$ , the H-OCO torsional potential exhibits a double well, with the equilibrium structures corresponding to  $\phi_{\text{HOCO}} = \pm 48^\circ$  and  $\pm 70.9^\circ$  for the  $\tilde{X}^2A$  and  $\tilde{A}^2A$  states, respectively. The multireference treatments of the  $\tilde{X}^2A$  state surface by both the Yarkony and Francisco groups results in an increase in the  $\phi_{\text{HOCO}}$  angle for the equilibrium  $\text{H}_2\text{C}(\text{OH})\text{O}^\bullet \tilde{X}^2A$  structure ( $\pm 59.6^\circ$  and  $\pm 57^\circ$ , respectively). Depending on the level of theory used with single reference methods, this dihedral angle for the equilibrium structure can range from  $\phi_{\text{HOCO}} = \pm 23^\circ$  (B3LYP/aug-cc-pVTZ) to  $\phi_{\text{HOCO}} = \pm 56^\circ$  (MP2/aug-cc-pVTZ). Like the anion, the *trans* configuration ( $\phi_{\text{HOCO}} \sim 180^\circ$ ) of the  $\tilde{X}^2A$  state of the neutral is much higher in energy than the *cis* configuration, and is separated from the global minimum by a very small barrier. In the neutral  $\tilde{A}^2A$  excited state, the *trans* configuration is higher in energy and unstable with respect to isomerization. In all cases, the relative stabilities of the *cis* and *trans* isomers arises from the stabilization of the *cis* isomer due to intramolecular interactions between the terminal oxygen (O1) and hydrogen (H3) atoms, as illustrated in the inset of Fig. 1. This interaction will be strongest in the anion, where the excess electron is localized on O1 leading to a stronger  $\text{O}^\bullet \dots \text{HO}$  ionic hydrogen bond.

The two equivalent minimum energy structures have  $C_1$  symmetry with  $\phi_{\text{HOCO}} = \pm 48^\circ$  or  $\pm 70.9^\circ$ , which are separated by a barrier in both the ground  $\tilde{X}^2A$  and excited  $\tilde{A}^2A$  state neutral electronic potential energy surfaces. A relaxed potential energy scan has a barrier to interconversion of  $158 \text{ cm}^{-1}$  for the ground  $\tilde{X}^2A$  state surface. This is lower than the multireference calculations from Dillon and Yarkony,<sup>26</sup> who report a barrier to interconversion of  $361 \text{ cm}^{-1}$  for the ground  $\tilde{X}^2A$  state, and with Eisfeld and Francisco, who report a barrier of at most  $550 \text{ cm}^{-1}$  for the  $\tilde{X}^2A$  state rotamer interconversion. The barrier to interconversion for the excited  $\tilde{A}^2A$  state is higher, at  $968 \text{ cm}^{-1}$ , which agrees very well with the

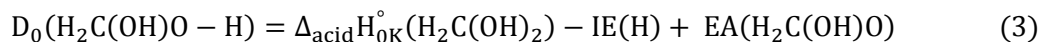
multireference calculations from Dillon and Yarkony (993 cm<sup>-1</sup>).<sup>26</sup> As mentioned previously, the vertical detachment region of the potential energy surface is what is accessed in the photoelectron detachment experiment performed here. In this region, the barrier lowers to only 50 cm<sup>-1</sup> for the ground  $\tilde{X}^2A$  state and 255 cm<sup>-1</sup> for the excited  $\tilde{A}^2A$  state. Based on the one-dimensional calculations of energies and wavefunctions for the H-OCO torsion performed using the potential cut shown in Fig. 1, we find that in the ground electronic state, the zero-point level lies 11 cm<sup>-1</sup> above the barrier to rotamer conversion, and the wavefunction has its largest amplitude at  $\phi_{\text{HOCO}} = 0^\circ$ . In the excited  $\tilde{A}^2A$  electronic state, there is still a barrier with respect to zero-point motion, and the ground vibrational state lies 99 cm<sup>-1</sup> below the barrier to free internal rotation. These conclusions agree well with those drawn by Dillon and Yarkony<sup>26</sup> based on their potential energy surfaces (which had all coordinates, besides  $\phi_{\text{HOCO}}$ , constrained to the equilibrium geometry of the anion)<sup>26</sup> and with Eisfeld and Francisco,<sup>11</sup> who excluded this coordinate from their work for this reason.

The consequences of the anion and the vibrationally averaged structure of neutral H<sub>2</sub>C(OH)O<sup>•</sup> both having C<sub>s</sub> symmetry leads to vibrational symmetry selection rules in the electronic spectra, resulting in vibrational modes  $\nu_{10}$  (in plane HCH rock),  $\nu_7$  (out of plane HCH rock), and  $\nu_2$  (HCH asymmetric stretch) not being active in the photoelectron spectrum (see Supplementary Material for mode description). Moreover, the selection rules of the torsional transitions are determined by the parity enforced by the symmetry of the potential, as emphasized by the double-headed arrows shown in Fig. 1. Because of the parity selection rules in the torsional coordinate, peak b is assigned as  $\nu_{12}(v''=0 \rightarrow v'=2)$ , or  $12_0^2$ . Based on the difference in peak positions between peak b and the EA, the neutral  $2\nu_{12}$  has a frequency of 220(10) cm<sup>-1</sup>. Peak a' is assigned as the anion-neutral sequence band  $\nu_{12}(v''=1 \rightarrow v'=1)$ , located 180(60) cm<sup>-1</sup> from the origin transition (peak a). Because the  $\nu_{12}$  fundamental frequency for either the anion or neutral cannot be measured directly, and the neutral H-OCO potential is highly anharmonic, the anion and neutral  $\nu_{12}$  fundamental frequencies cannot be directly obtained from the measured  $2\nu_{12}$  overtone or the position of the  $\nu_{12}(v''=1 \rightarrow v'=1)$  sequence band.

We can, however, use a combination of the calculated anion fundamental frequency  $\nu_{12}(v''=0 \rightarrow v''=1) = 269 \text{ cm}^{-1}$  from the anion torsional potential energy surface (which is well-described as a harmonic oscillator near its equilibrium structure) in combination with the experiment to derive the  $\nu_{12}$  fundamental frequencies. Using the calculated  $\nu_{12}(v''=0 \rightarrow v''=1)$  and the position of the  $\nu_{12}(v''=1 \rightarrow v''=1)$  sequence band in relation to the EA, the neutral  $\nu_{12}$  fundamental frequency  $\nu_{12}(v' = 0 \rightarrow v' = 1) = 90(60) \text{ cm}^{-1}$ . By comparison, the calculated neutral  $\nu_{12}$  fundamental frequency ( $92.3 \text{ cm}^{-1}$ ) is very close to this value, which is calculated using the one-dimensional potential shown in Fig. 1 (based on the relaxed geometries of the anion). When a relaxed scan of the neutral  $\tilde{X}^2A$  torsional potential energy surface is used instead, this frequency drops to  $36.7 \text{ cm}^{-1}$  due to the larger barrier along this cut of the potential. This comparison further validates the approximations made in the treatment of the torsional mode. In addition, using this in combination with the measured neutral  $2\nu_{12}$ ,  $\nu_{12}(v' = 1 \rightarrow v' = 2) = 130(60) \text{ cm}^{-1}$  for  $\text{H}_2\text{C}(\text{OH})\text{O}^\bullet$ . The error bars on these frequencies are defined by the experimental error bars on the peak positions. This can be compared to the calculated values of  $170 \text{ cm}^{-1}$  for the neutral  $\tilde{X}^2A$  potential energy curve calculated at the anion relaxed scan geometries (as shown in Fig. 1) and  $155 \text{ cm}^{-1}$  for the neutral  $\tilde{X}^2A$  relaxed surface. Unfortunately, this type of analysis and comparison of experiment with theory for the  $\text{H}_2\text{C}(\text{OH})\text{O}^\bullet \tilde{A}^2A$  torsional frequency is not possible. The torsional frequency for  $\text{H}_2\text{C}(\text{OH})\text{O}^\bullet \tilde{A}^2A$  could not be measured due to the highly spectrally congested spectrum (including spectral overlap with detachment to the ground  $\tilde{X}^2A$  state) and the relatively low-resolution of the spectrum shown in Fig. 2.

### ***B. Methanediol Thermochemistry***

The measurement of the EAs of molecules can provide information about the gas phase chemistry of their protonated counterpart with the use of a thermochemical cycle. The thermochemical cycle for methanediol is described by Eq. 3:



Here, the EA of  $\text{H}_2\text{C}(\text{OH})\text{O}^\bullet$  is experimentally determined as 2.220(2) eV or 51.19(5) kcal mol<sup>-1</sup>. The ionization energy of atomic hydrogen (IE(H)=313.59 kcal mol<sup>-1</sup>) is known.<sup>52</sup> With this equation, either the O–H bond dissociation energy,  $D_0(\text{H}_2\text{C}(\text{OH})\text{O–H})$ , or the gas phase deprotonation enthalpy,  $\Delta_{\text{acid}}\text{H}^\circ_{0\text{K}}(\text{H}_2\text{C}(\text{OH})_2)$ , of methanediol can be obtained. Since there is no experimental measurement of either of these quantities, quantum chemical calculations must be relied upon to obtain one of these values. In this instance, the  $\Delta_{\text{acid}}\text{H}^\circ_{0\text{K}}(\text{H}_2\text{C}(\text{OH})_2)$  was chosen since this quantity only depends on calculating formation enthalpies of closed shell species, namely  $\text{H}_2\text{C}(\text{OH})\text{O}^-$ ,  $\text{H}_2\text{C}(\text{OH})_2$ , and  $\text{H}^+$ . Here, the G4 composite method was used yielding  $\Delta_{\text{acid}}\text{H}^\circ_{0\text{K}}(\text{H}_2\text{C}(\text{OH})_2) = 366$  kcal mol<sup>-1</sup>. Other composite methods were also used and verified this result, specifically CBS-APNO (366.4 kcal mol<sup>-1</sup>) and CBS-QB3 (365.7 kcal mol<sup>-1</sup>). Since the predicted uncertainty in these calculations is on the order of 0.8 to 1.5 kcal mol<sup>-1</sup>, this results in  $D_0(\text{H}_2\text{C}(\text{OH})\text{O–H}) = 104(2)$  kcal mol<sup>-1</sup>, using a conservative estimate of the uncertainty. A previously calculated O–H bond dissociation energy<sup>53</sup> of 102.7 kcal mol<sup>-1</sup> is in excellent agreement with our semi-empirical value.

### ***C. Photodetachment Producing $\text{H}_2\text{C}(\text{OH})\text{O}^\bullet \tilde{X}^2A$ and $\tilde{A}^2A$ Electronic States***

While it is tempting to compare the photoelectron spectrum of  $\text{H}_2\text{C}(\text{OH})\text{O}^-$  with those of other alkoxy anions, such as methoxide ( $\text{CH}_3\text{O}^-$ ) and ethoxide ( $\text{H}_2\text{C}(\text{CH}_3)\text{O}^-$ ), this would not be a fair comparison, especially with respect to the Jahn-Teller coupling that was essential for a proper interpretation of the methoxide and ethoxide photoelectron spectra. There, the substitution of a methyl group from methoxy to ethoxy was seen as a perturbation of the Jahn-Teller distortion, and an accordingly strong coupling and small energy difference between the neutral radical ground and first excited electronic states. However, the substitution of a hydroxyl group drastically changes the electronic structure and any neutral ground/excited electronic state coupling, as described by Dillon and Yarkony.<sup>26</sup> Experimentally, there is at least an order of magnitude larger energy difference between the ground and first excited electronic states in hydroxymethoxy compared to ethoxy. While there is still significant coupling between the ground and first excited electronic states in hydroxymethoxy, exemplified by a low-

lying seam of conical intersection, there are substantial differences in the topology of the electronic state surfaces of hydroxymethoxy compared to the classic Jahn-Teller topology found in the electronic structure of methoxy radical (or even in the pseudo Jahn-Teller ethoxy radical). See Reference <sup>26</sup> for a thorough discussion on the topic.

The photoelectron simulation of detachment forming  $\text{H}_2\text{C}(\text{OH})\text{O}^* \tilde{A}^2A$  captures the experimental data very well (Fig. 2). The differences between the experiment and simulation likely differ mostly due to the separable harmonic treatment employed here. However, it would be interesting if there is any additional broadening or spectral congestion in the high eBE portion of the photoelectron spectrum that could be due to any nonadiabatic coupling between the two electronic states of the neutral. Interestingly, Dillon and Yarkony found that there is a significant dependence on the  $\phi_{\text{HOCO}}$  torsion coordinate for the energy of the seam of conical intersection between the two states, ranging from  $\sim 0.38$  eV to  $\sim 0.53$  eV above the ground electronic state minimum.<sup>26</sup> This is energetically accessible in the experiments performed here. However, whether or not photodetachment accesses these regions of strong coupling on the neutral potential energy surfaces is unknown. While the calculation used here certainly matches the experimental spectrum qualitatively, a more detailed calculation including the possible effects of nonadiabatic coupling would be interesting.

## VI. Conclusions

Photodetachment of the hydroxymethoxide anion,  $\text{H}_2\text{C}(\text{OH})\text{O}^-$ , with 355 nm photons forms the ground ( $\tilde{X}^2A$ ) and first excited ( $\tilde{A}^2A$ ) states of  $\text{H}_2\text{C}(\text{OH})\text{O}^*$ . The photoelectron spectrum provides the electron affinity of  $\text{H}_2\text{C}(\text{OH})\text{O}^*$  ( $\text{EA} = 2.220(2)$  eV), together with the measurement of several vibrational frequencies of the hydroxymethoxy radical in its  $\tilde{X}^2A$  electronic state. The  $\tilde{A}^2A$  excited state spectrum is characterized by a long vibrational progression which results in a mostly unstructured photoelectron spectrum with an  $\tilde{X} \rightarrow \tilde{A}$  excitation term energy of  $\sim 0.4$  eV. Franck-Condon activity in specific vibrational modes is indicative of a change in the equilibrium structures between the anion and neutral

states. The H-OCO torsion is one of the main active vibrations in the spectra, along with overtones and combination bands of the OCO stretching and HOC bending/CH<sub>2</sub> wagging vibrations. Motion along the neutral H-OCO torsional double-well potentials is not well described by the harmonic oscillator approximation and hence requires explicit treatment to calculate the associated Franck-Condon factors, unlike the other vibrational modes. The resulting calculated photoelectron spectra for detachment to both ground  $\tilde{X}^2A$  and excited  $\tilde{A}^2A$  states show good agreement with the experimental data, supporting the interpretation of the spectra. Because of the agreement between calculation and experiment, the inclusion of nonadiabatic vibronic coupling between the electronic states of hydroxymethoxy does not appear to be necessary to reproduce accurately the experimental photoelectron spectrum. This observation further separates hydroxymethoxy from other small substituted alkoxy radicals, such as ethoxy (H<sub>2</sub>C(CH<sub>3</sub>)O<sup>•</sup>), in which the inclusion of vibronic coupling was crucial to simulating the experimental photoelectron spectrum.

### Supplementary Material

See Supplementary Material at URL for additional information regarding the calculations and analysis.

### Acknowledgments

W.C.L. gratefully acknowledges significant contributions for this work from NSF Chemistry (CHE1213862), NSF Physics Frontier Center (PHY1125844), and AFOSR (Grant FA9550-12-1-0125).

A.B.M acknowledges support from NSF Chemistry (CHE1619660).

### References

- <sup>1</sup> J. J. Orlando, G. S. Tyndall and T. J. Wallington, *Chem. Rev.* **103**, 4657 (2003).
- <sup>2</sup> P. Devolder, *J. Photochem. Photobio.* **157**, 137 (2003).
- <sup>3</sup> R. Atkinson, *Atmos. Environ.* **41**, 8468 (2007).
- <sup>4</sup> C. C. Carter, J. R. Atwell, S. Gopalakrishnan and T. A. Miller, *J. Phys. Chem. A* **104**, 9165 (2000).
- <sup>5</sup> H. J. Curran, *Int. J. Chem. Kinet.* **38**, 250 (2006).
- <sup>6</sup> H. J. Curran, P. Gaffuri, W. J. Pitz and C. K. Westbrook, *Combust. Flame* **114**, 149 (1998).
- <sup>7</sup> A. C. Davis and J. S. Francisco, *J. Phys. Chem. A* **118**, 10982 (2014).

- <sup>8</sup> M. L. Weichman, J. B. Kim and D. M. Neumark, *J. Phys. Chem. A* **119**, 6140 (2015).
- <sup>9</sup> P. Neeb, F. Sauer, O. Horie and G. K. Moortgat, *Atmos. Environ.* **31**, 1417 (1997).
- <sup>10</sup> L. Vereecken and J. S. Francisco, *Chem. Soc. Rev.* **41**, 6259 (2012).
- <sup>11</sup> W. Eisfeld and J. S. Francisco, *J. Chem. Phys.* **131**, 134313 (2009).
- <sup>12</sup> S. Bauerle and G. K. Moortgat, *Chem. Phys. Lett.* **309**, 43 (1999).
- <sup>13</sup> J. S. Francisco and W. Eisfeld, *J. Phys. Chem. A* **113**, 7593 (2009).
- <sup>14</sup> C. Barrientos, P. Redondo, H. Martinez and A. Largo, *Astrophys. J.* **784**, 132 (2014).
- <sup>15</sup> F. Duvernay, G. Danger, P. Theule, T. Chiavassa and A. Rimola, *Astrophys. J.* **791**, 75 (2014).
- <sup>16</sup> B. M. Hays and S. L. W. Weaver, *J. Phys. Chem. A* **117**, 7142 (2013).
- <sup>17</sup> D. R. Kent, S. L. Widicus, G. A. Blake and W. A. Goddard, *J. Chem. Phys.* **119**, 5117 (2003).
- <sup>18</sup> F. Duvernay, A. Rimola, P. Theule, G. Danger, T. Sanchez and T. Chiavassa, *Phys. Chem. Chem. Phys.* **16**, 24200 (2014).
- <sup>19</sup> M. Baker and W. Gabryelski, *Int. J. Mass Spectrom.* **262**, 128 (2007).
- <sup>20</sup> A. Simakov, G. B. S. Miller, A. J. C. Bunkan, M. R. Hoffmann and E. Uggerud, *Phys. Chem. Chem. Phys.* **15**, 16615 (2013).
- <sup>21</sup> Q. Cao, S. Berski, Z. Latajka, M. Rasanen and L. Khriachtchev, *Phys. Chem. Chem. Phys.* **16**, 5993 (2014).
- <sup>22</sup> T. M. Ramond, G. E. Davico, R. L. Schwartz and W. C. Lineberger, *J. Chem. Phys.* **112**, 1158 (2000).
- <sup>23</sup> J. J. Dillon and D. R. Yarkony, *J. Chem. Phys.* **131**, 134303 (2009).
- <sup>24</sup> J. J. Dillon and D. R. Yarkony, *J. Chem. Phys.* **130**, 154312 (2009).
- <sup>25</sup> D. M. Neumark, *J. Phys. Chem. A* **112**, 13287 (2008).
- <sup>26</sup> J. Dillon and D. R. Yarkony, *J. Chem. Phys.* **137**, 154315 (2012).
- <sup>27</sup> J. Jin, I. Sioutis, G. Tarczay, S. Gopalakrishnan, A. Bezant and T. A. Miller, *J. Chem. Phys.* **121**, 11780 (2004).
- <sup>28</sup> G. B. Ellison, P. C. Engelking and W. C. Lineberger, *J. Phys. Chem.* **86**, 4873 (1982).
- <sup>29</sup> L. Sheps, E. M. Miller and W. C. Lineberger, *J. Chem. Phys.* **131**, 064304 (2009).
- <sup>30</sup> Y. J. Lu, J. H. Lehman and W. C. Lineberger, *J. Chem. Phys.* **142**, 044201 (2015).
- <sup>31</sup> P. Ho, D. J. Bamford, R. J. Buss, Y. T. Lee and C. B. Moore, *J. Chem. Phys.* **76**, 3630 (1982).
- <sup>32</sup> R. Spence and W. Wild, *J. Chem. Soc.* **1**, 506 (1935).
- <sup>33</sup> V. Dribinski, A. Ossadtchi, V. A. Mandelstam and H. Reisler, *Rev. Sci. Instrum.* **73**, 2634 (2002).
- <sup>34</sup> B. Dick, *Phys. Chem. Chem. Phys.* **16**, 570 (2014).
- <sup>35</sup> C. Blondel, W. Chaibi, C. Delsart, C. Drag, F. Goldfarb and S. Kroger, *European Physical Journal D* **33**, 335 (2005).
- <sup>36</sup> H. Hotop and W. C. Lineberger, *J. Phys. Chem. Ref. Data* **14**, 731 (1985).
- <sup>37</sup> J. R. Smith, J. B. Kim and W. C. Lineberger, *Phys. Rev. A* **55**, 2036 (1997).
- <sup>38</sup> J. Cooper and R. N. Zare, *J. Chem. Phys.* **48**, 942 (1968).
- <sup>39</sup> A. Sanov, *Annu. Rev. Phys. Chem.* **65**, 341 (2014).
- <sup>40</sup> M. J. Frisch, G. W. Trucks, H. B. Schlegel, G. E. Scuseria, M. A. Robb, J. R. Cheeseman, G. Scalmani, V. Barone, B. Mennucci, G. A. Petersson, H. Nakatsuji, M. Caricato, X. Li, H. P. Hratchian, A. F. Izmaylov, J. Bloino, G. Zheng, J. L. Sonnenberg, M. Hada, M. Ehara, K. Toyota, R. Fukuda, J. Hasegawa, M. Ishida, T. Nakajima, Y. Honda, O. Kitao, H. Nakai, T. Vreven, J. A. Montgomery Jr., J. E. Peralta, F. Ogliaro, M. J. Bearpark, J. Heyd, E. N. Brothers, K. N. Kudin, V. N. Staroverov, R. Kobayashi, J. Normand, K. Raghavachari, A. P. Rendell, J. C. Burant, S. S. Iyengar, J. Tomasi, M. Cossi, N. Rega, N. J. Millam, M. Klene, J. E. Knox, J. B. Cross, V. Bakken, C. Adamo, J. Jaramillo, R. Gomperts, R. E. Stratmann, O. Yazyev, A. J. Austin, R. Cammi, C. Pomelli, J. W. Ochterski, R. L. Martin, K. Morokuma, V. G. Zakrzewski, G. A. Voth, P. Salvador, J. J. Dannenberg, S. Dapprich, A. D. Daniels, Ö. Farkas, J. B. Foresman, J. V. Ortiz, J. Cioslowski and D. J. Fox; Gaussian, Inc.: Wallingford, CT, USA, 2009.
- <sup>41</sup> K. M. Ervin, T. M. Ramond, G. E. Davico, R. L. Schwartz, S. M. Casey and W. C. Lineberger, *J. Phys. Chem. A* **105**, 10822 (2001).
- <sup>42</sup> K. M. Ervin, J. Ho and W. C. Lineberger, *J. Phys. Chem.* **92**, 5405 (1988).

- <sup>43</sup> T. E. Sharp and H. M. Rosenstock, *J. Chem. Phys.* **41**, 3453 (1964).
- <sup>44</sup> K. M. Vogelhuber, S. W. Wren, A. B. McCoy, K. M. Ervin and W. C. Lineberger, *J. Chem. Phys.* **134**, 184306 (2011).
- <sup>45</sup> J. H. Frederick and C. Woywod, *J. Chem. Phys.* **111**, 7255 (1999).
- <sup>46</sup> Y. C. Zhao, B. X. Wang, H. Y. Li and L. Wang, *Journal of Molecular Structure - Theochem* **818**, 155 (2007).
- <sup>47</sup> S. J. Blanksby, T. M. Ramond, G. E. Davico, M. R. Nimlos, S. Kato, V. M. Bierbaum, W. C. Lineberger, G. B. Ellison and M. Okumura, *J. Am. Chem. Soc.* **123**, 9585 (2001).
- <sup>48</sup> D. J. Goebbert, K. Pichugin and A. Sanov, *J. Chem. Phys.* **131**, 164308 (2009).
- <sup>49</sup> P. C. Engelking, *J. Phys. Chem.* **90**, 4544 (1986).
- <sup>50</sup> E. P. Wigner, *Physical Review* **73**, 1002 (1948).
- <sup>51</sup> W. C. Lineberger and B. W. Woodward, *Phys. Rev. Lett.* **25**, 424 (1970).
- <sup>52</sup> U. D. Jentschura, S. Kotochigova, E. O. LeBigot, P. J. Mohr and B. N. Taylor, *The Energy Levels of Hydrogen and Deuterium (version 2.1)*. Available: <http://physics.nist.gov/PhysRefData/HDEL/energies.html>. National Institute of Standards and Technology, Gaithersburg, MD, 2016.
- <sup>53</sup> C. K. Huang, Z. F. Xu, M. Nakajima, H. M. T. Nguyen, M. C. Lin, S. Tsuchiya and Y. P. Lee, *J. Chem. Phys.* **137** (2012).

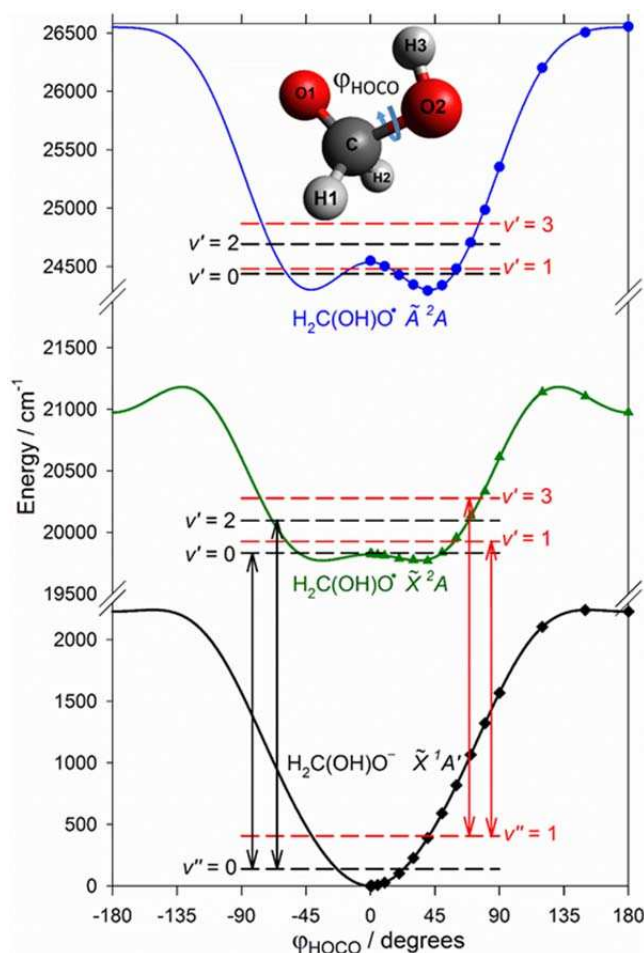


**Figure 1:** Calculated (CCSD(T)/aug-cc-pVTZ) 1D potential energy curves of the torsional coordinate of  $\text{H}_2\text{C(OH)O}^- \tilde{X}^1A'$  (black),  $\text{H}_2\text{C(OH)O}^\bullet \tilde{X}^2A$  (green), and  $\text{H}_2\text{C(OH)O}^\bullet \tilde{A}^2A$  (blue) states important in the photodetachment process. The anion potential energy surface was calculated by varying the  $\phi_{\text{HOCO}}$  dihedral angle while allowing the remaining coordinates to be optimized (referred to as a relaxed scan). The neutral surfaces were constructed by calculating the energy of the neutral molecule ( $\tilde{X}^2A$  and  $\tilde{A}^2A$  states) at the optimized anion geometries, referred to as the vertical potential energy curves, which represent the region of the potential energy surfaces important to photodetachment. The dashed horizontal lines represent the eigenvalues of these potentials, while their colors, together with the double headed arrows between the anion and neutral ground states, represent the parity allowed transitions. The calculated (CCSD(T)/aug-cc-pVTZ) structure of the hydroxymethoxide anion is also shown with the atom numbering and the dihedral angle,  $\phi_{\text{HOCO}}$ , referred to in the text.

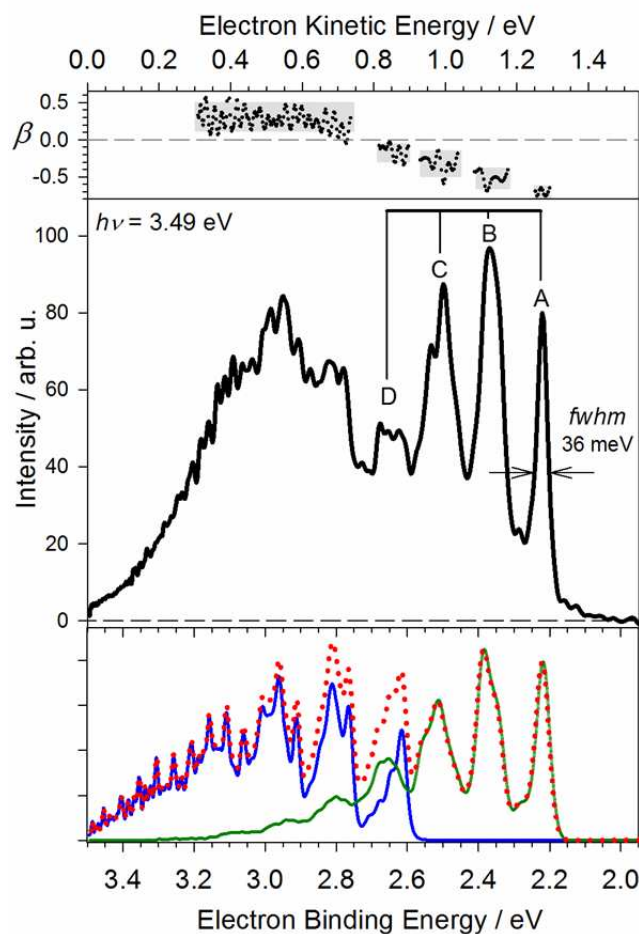


**Figure 2, Middle panel:** Experimental photoelectron spectrum of  $\text{H}_2\text{C}(\text{OH})\text{O}^-$ , using 3.49 eV (355 nm) photon energy. Peaks A through D are discussed in the text. **Upper panel:** Experimental anisotropy parameters ( $\beta$ ) as a function of electron kinetic energy. The black circles are a series of  $\beta$  measured above the *fwhm* of each resolvable peak in the spectrum across each peak. The grey shaded regions indicate the average  $\beta$ , where the height shows the scatter of the  $\beta$  values across this width. **Lower panel:** Convolved photoelectron simulations of detachment to the ground (green) and excited (blue) electronic states of  $\text{H}_2\text{C}(\text{OH})\text{O}^-$ , along with their sum (red dots).

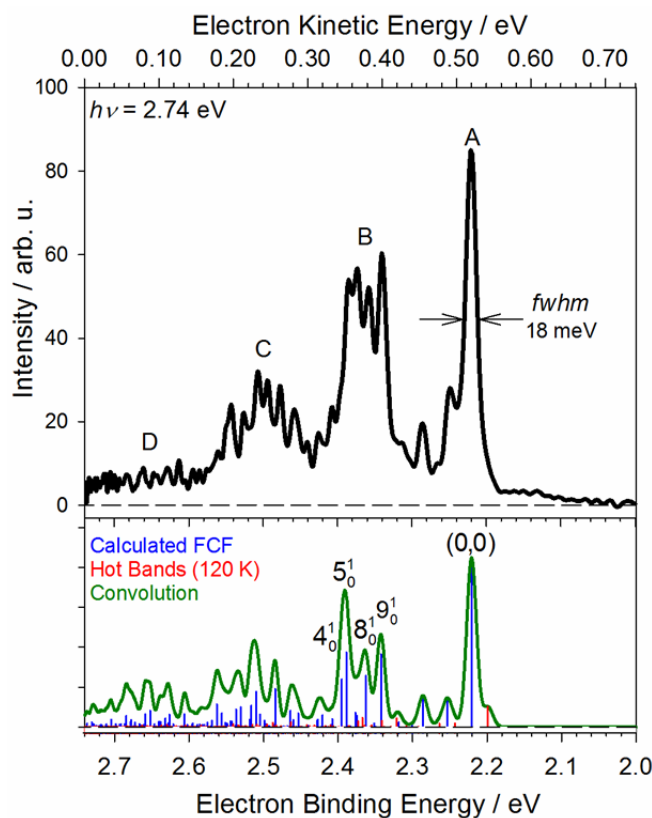


**Figure 3, Upper panel:** Experimental photoelectron spectrum of  $\text{H}_2\text{C}(\text{OH})\text{O}^-$  using 2.74 eV (453 nm) photon energy. The letters A through D are the same labels shown in Fig. 1. **Lower panel:** Calculated (CCSD(T)/aug-cc-pVTZ) Franck-Condon factors (sticks) and convolved simulation (blue trace). The green sticks represent transitions from the vibrational ground state of the anion while the red sticks are vibrational hot bands, *i.e.* transitions from an excited vibrational state of the anion. The calculated stick spectrum was convolved with Gaussian functions of varying *fwhm* in order to match the measured experimental resolution.

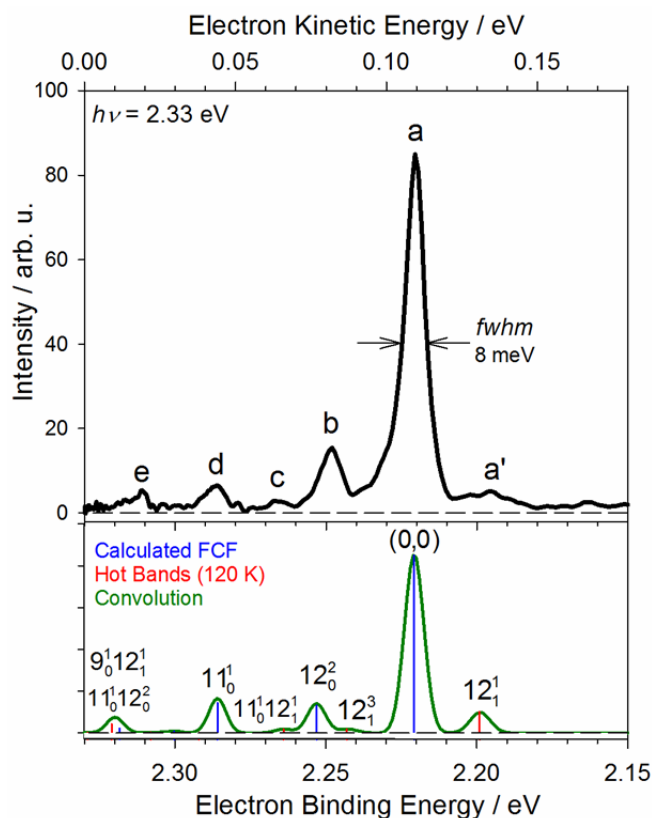


**Figure 4:** **TOP** Photoelectron spectrum of  $\text{H}_2\text{C}(\text{OH})\text{O}^-$  using 2.33 eV (532 nm) photon energy. Peaks a–e are described in the text. **BOTTOM** Calculated (CCSD(T)/aug-cc-pVTZ) Franck-Condon factors (sticks) and convolved simulation (blue trace) with assigned transitions. The green sticks correspond to transitions originating from the vibrational ground state of the anion, while the red sticks correspond to transitions with one quantum of excitation in a low frequency torsional ( $\nu_{12}$ ) mode of the anion. See text and Supplemental Material for details.

**Table 1:** Calculated minimum energy structure of  $\text{H}_2\text{C}(\text{OH})\text{O}^- \tilde{X}^1A'$  (CCSD(T)/aug-cc-pVTZ),  $\text{H}_2\text{C}(\text{OH})\text{O} \cdot \tilde{X}^2A$  (ROCCSD(T)/aug-cc-pVTZ), and  $\text{H}_2\text{C}(\text{OH})\text{O} \cdot \tilde{A}^2A$  (CIS/aug-cc-pVTZ), as well as the difference between structural parameters of the anion and neutral structures ( $\Delta = \text{anion structure} - \text{neutral structure}$ ). Figure 1 shows the atom numbering used in this work. The values in boldface show the largest geometry changes. These calculated geometries agree well with the values in Refs. <sup>11</sup> and <sup>26</sup>.

| Parameter  | Anion<br>( $\tilde{X}^1A'$ ) | Neutral<br>( $\tilde{X}^2A$ ) | $\Delta$     | Neutral<br>( $\tilde{A}^2A$ ) | $\Delta$     |
|--|------------------------------|-------------------------------|--------------|-------------------------------|--------------|
| $r_{\text{CH}_1} / \text{\AA}$                       | 1.121                        | 1.111                         | 0.01         | 1.084                         | 0.037        |
| $r_{\text{CH}_2} / \text{\AA}$                       | 1.121                        | 1.099                         | 0.021        | 1.08                          | 0.041        |
| $r_{\text{CO}_1} / \text{\AA}$                       | 1.317                        | 1.349                         | -0.032       | 1.402                         | -0.085       |
| <b><math>r_{\text{CO}_2} / \text{\AA}</math></b>     | <b>1.513</b>                 | <b>1.405</b>                  | <b>0.108</b> | <b>1.375</b>                  | <b>0.138</b> |
| $r_{\text{OH}_3} / \text{\AA}$                       | 0.967                        | 0.964                         | 0.003        | 0.941                         | 0.026        |
| $\angle_{\text{H}_1\text{CH}_2} / ^\circ$            | 107                          | 107                           | 0            | 110.5                         | -3.5         |
| $\angle_{\text{O}_1\text{CO}_2} / ^\circ$            | <b>111.7</b>                 | <b>116.5</b>                  | <b>-4.8</b>  | <b>107.5</b>                  | <b>4.2</b>   |
| $\angle_{\text{O}_2\text{CH}_3} / ^\circ$            | <b>96.8</b>                  | <b>107.7</b>                  | <b>-10.9</b> | <b>110.5</b>                  | <b>-13.7</b> |
| $\varphi_{\text{H}_3\text{O}_2\text{CO}_1} / ^\circ$ | <b>0</b>                     | <b>47.6</b>                   | <b>-47.6</b> | <b>70.9</b>                   | <b>-70.9</b> |

**Table 2:** Summary of the major results. The calculated results are based on the CCSD(T)/aug-cc-pVTZ (EA and vibrational frequencies) and the G4 composite method (gas phase acidity).

|  | Experiment          | Calculation <sup>b</sup> |
|--|---------------------|--------------------------|
| Electron affinity / eV   | 2.220(2)            | 2.19                     |
| $\Delta_{\text{acid}}H_{0\text{K}}^{\circ}(\text{H}_2\text{C}(\text{OH})_2) / \text{kcal mol}^{-1}$                            | -                   | 366(2)                   |
| $\Delta_{\text{acid}}H_{298\text{K}}^{\circ}(\text{H}_2\text{C}(\text{OH})_2) / \text{kcal mol}^{-1}$                          | -                   | 367(2)                   |
| $D_0(\text{H}_2\text{C}(\text{OH})\text{O}-\text{H}) / \text{kcal mol}^{-1}$   | 104(2) <sup>a</sup> |                          |
| $\text{H}_2\text{C}(\text{OH})\text{O}^{\cdot} \tilde{X}^2A$ Vibrational Frequencies / $\text{cm}^{-1}$                        |                     |                          |
| $2\nu_{12}$  | 220(10)             | 261                      |
| $\nu_{11}$   | 530(10)             | 526                      |
| $\nu_9$  | 960(50)             | 982                      |
| $\nu_8$  | 1110(50)            | 1146                     |
| <sup>a</sup> Determined based on experimental and calculated quantities through the thermochemical cycle shown in Eq. 3        |                     |                          |
| <sup>b</sup> Calculated values are based on harmonic vibrational frequencies, except for $\nu_{12}$ , as discussed in the text |                     |                          |